AN ELECTRO-OPTICAL PROCESSOR FOR OPTIMAL CONTROL

David Casasent, Charles Neuman and Mark Carlotto*

Department of Electrical Engineering, Carnegie-Mellon University
Pittsburgh, Pennsylvania 15213
*Present Address: The Analytical Sciences Corporation
1 Jacob Way, Reading, Massachusetts 01867

ABSTRACT

An iterative optical processor (IOP) that can solve iteratively systems of simultaneous linear algebraic equations is described. Modifications to the system enable it to solve the algebraic Riccati equation and the linear-quadratic-regulator (LQR) problem of optimal control. We describe the resulting electro-optical processor and illustrate how we implement the Richardson and modified Kleinman algorithms to solve the LQR problem.

1. INTRODUCTION

Applications of optimal control will continue to grow in complexity as advanced sensors [1-2] with improved accuracy emerge and as redundant sensors are incorporated to improve the reliability of the system being controlled. We describe (in Section 2) an iterative optical processor (IOP)[3] that can be used for such advanced optimal control applications. The specific case study chosen (in Section 3) was the calculation of the optimal control signals for the F100 turbofan jet engine [4-6]. In Section 4, we describe how the IOP can be used to solve the algebraic Riccati equation (ARE) of the linear quadratic regulator (LQR) problem [7-8] of modern control engineering. We do so by implementing the Richardson [9] and a modified Kleinman [10] algorithms. Preliminary experimental results are then given in Section 5.

2. ITERATIVE OPTICAL PROCESSOR

A schematic diagram of the IOP is shown in Figure 1. The system's input at plane P_1 is a linear array of light emitting diodes (LEDs) or laser diodes. We denote their outputs at iteration j by the row vector $\underline{x}^T(j)$, with elements x_m, where the superscript T denotes transpose. The light leaving P_1 is imaged vertically and expanded horizontally to illuminate a mask at P_2 whose transmittance is described by a matrix $\underline{H}^T$ with elements h_{mn}. The light leaving P_2 is imaged horizontally and collected vertically on an output linear photodetector array at P_3. We denote the P_3 output at iteration j by the row vector $\underline{c}^T(j)$ with elements c_n. The system output is thus

$$\underline{c}^T(j) = \underline{x}^T(j)\underline{H}^T \tag{1}$$

and its elements are given by

$$c_n = \sum_{m=1}^{M} x_m h_{mn}. \tag{2}$$

For notational simplicity, we will not specifically denote the transposed vectors and matrices in the system and we will thus describe the system output at P_3 by

$$\underline{c}(j) = \underline{H}\,\underline{x}(j), \tag{3a}$$

whose elements are given by

$$c_n = \sum_{m=1}^{M} x_m h_{mn}. \tag{3b}$$

From (3), we see that this optical system realizes a vector-matrix product as first described in [11].

In [3], we modified this system to include addition of an exogenous vector to the P_3 output and feedback of the sum to the input as the new $\underline{x}(j+1)$ iterate. In Figure 1, we modify the system further by: forming the difference between the $\underline{H}\,\underline{x}(j)$ output in (3) and a fixed exogenous vector $\underline{y}$, multiplying this difference by an acceleration parameter ω, and adding the result to the previous input vector $\underline{x}(j)$ to yield the next $\underline{x}(j+1)$ iterate. The new system of Figure 1 thus realizes the Richardson algorithm [9]

$$\underline{x}(j+1) = \underline{x}(j) + \omega[\underline{y} - \underline{H}\,\underline{x}(j)]. \tag{4}$$

In the control applications to be addressed (in Section 3), the elements of all vectors and matrices are bipolar. Since the light output leaving P_1, the transmittance of the mask

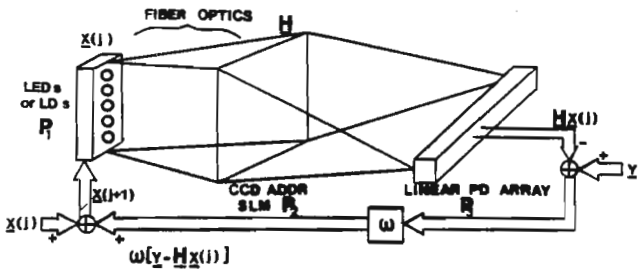

FIGURE 1. Schematic diagram of the iterative optical processor (IOP)

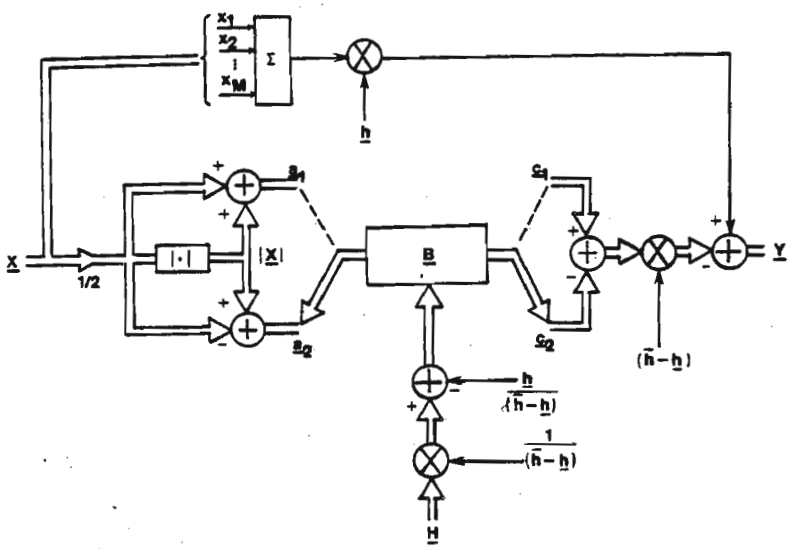

FIGURE 2. Schematic diagram of the bipolar vector-matrix multiplier

FIGURE 3. Photograph of the laboratory iterative optical processor (IOP)

Casasent 2

at P_2, and the photodetector's outputs at P_3 must be real and positive, we modified the system to allow it to operate on bipolar data. We denote the bipolar algebraic variables describing the input, mask and added exogenous vector by $\underline{x}$, $\underline{H}$ and $\underline{y}$ as in (4). We denote vectors by underlined lower-case letters, matrices by underlined capital letters and scalars by a single lower-case letter (usually Greek). The variables in the optical system are denoted by $\underline{a}$, $\underline{B}$ and $\underline{c}$. For the P_2 mask, we scale and bias the matrix $\underline{H}$ such that the elements of the matrix $\underline{B}$ used at P_2 in the system are

$$b_{mn} = (h_{mn} - \underline{h})/\bar{h} - \underline{h}), \tag{5}$$

where $\bar{h}$ and $\underline{h}$ are the values of the maximum and minimum elements of $\underline{H}$. From (5), we find that $0 \leq b_{mn} \leq 1$ and thus that the transmittances of the optical mask lie between 0 and 1 as required. To handle bipolar data, we decompose each element of the bipolar input vector $\underline{x}$ into its positive $\underline{x}^+$ and negative $\underline{x}^-$ components. For the optical inputs, we have

$$\begin{aligned} a_{1m} &\equiv 0.5(x_m + |x_m|) \\ a_{2m} &\equiv 0.5(x_m - |x_m|) \end{aligned} \tag{6}$$

for $m = 1,\ldots,M$. In this form, $\underline{a}_1 = \underline{x}^+$ and $\underline{a}_2 = \underline{x}^-$ are both real and positive. To obtain the desired bipolar output vector, the system is operated twice with inputs $\underline{a}_1$ and $\underline{a}_2$. The two outputs $\underline{B}\,\underline{a}_1$ and $\underline{B}\,\underline{a}_2$ are subtracted, scaled and biased (by the electronic feedback system) to yield

$$\underline{y} = \underline{H}\,\underline{x} = (\bar{h} - \underline{h})[\underline{B}\,\underline{a}_1 - \underline{B}\,\underline{a}_2] + \underline{h}\sum_{m=1}^{M} x_m(1\ldots.1)^T. \tag{7}$$

A schematic diagram of the bipolar vector-matrix processor is shown in detail in Figure 2. For simplicity, we will not include the associated scaling, biasing and post-processing details associated with the operation on bipolar data in future system descriptions. For the acceleration parameter ω, we choose $\omega = -1/\lambda_{max}$, where λ_{max} is the absolute value of the largest eigen-value of $\underline{H}$. In practice, we estimate λ_{max} from the Euclidean norm of the matrix $\underline{H}$ as in [12].

We have fabricated a laboratory prototype of the IOP using 10 LED inputs, a 10 × 10 film mask and a parallel readout linear detector array. A microprocessor, arithmetic logic unit, multiplier and memory in the feedback network provide the necessary control and post-processing. Correction for spatial non-uniformities in the LED inputs and responsivities of the output photodetector elements are made by ROMs in the electronic feedback system. A residual system spatial uniformity of 0.8% was measured. The interconnection between P_1 and P_2 was achieved by a specially fabricated fiber-optic system. The vertical size of the mask was 4 mm. It was chosen to match the height of the detector elements so that planes P_2 and P_3 could be placed in direct contact. These fiber-optic interconnections assured uniform illumination of each row of P_2 and eliminated cross-talk between rows. This also resulted in a rugged system of small size and weight. A photograph of the resultant processor is shown in Figure 3. The total length of the system is less than 5 cm.

3. F100 TURBOFAN JET ENGINE CASE STUDY

The specific LQR problem we consider is the calculation of the optimal control signals $\underline{u}(t)$ for the F100 turbofan jet engine. With the help of NASA-Lewis Research Center, we obtained state $\underline{F}$ and control distribution $\underline{G}$ matrices which model the engine and state $\underline{Q}$ and control $\underline{R}$ weighting matrices for the LQR control system designs. We thus compiled the requisite data [$\underline{F}$, $\underline{G}$, $\underline{Q}$, $\underline{R}$] for LQR control system designs of various orders (N = 18, 5 and 3) for each of the six regimes in the flight envelope.

The LQR problem [7] of modern control engineering is to find the control signals $\underline{u}(t)$ that minimize the quadratic cost performance index

$$J[\underline{u}(t)] = 0.5\int_0^\infty [\underline{x}^T(t)\underline{Q}\,\underline{x}(t) + \underline{u}^T(t)\underline{R}\,\underline{u}(t)]\,dt \tag{8}$$

for the linearized system model

$$\frac{d\underline{x}}{dt} = \underline{F}\,\underline{x}(t) + \underline{G}\,\underline{u}(t), \tag{9}$$

where $\underline{x}(t)$ is an N × 1 state vector and $\underline{u}(t)$ is an M × 1 control vector. In (8), $\underline{Q}$ is an N × N weighting matrix and $\underline{R}$ is an M × M weighting matrix which measure the cost of state errors and applied control, respectively. In (9), $\underline{F}$ is the N × N state matrix and $\underline{G}$ is the N × M control distribution matrix which model the open-loop dynamic response of the F100 engine.

The solution to the LQR problem is the M × N LQR feedback gain matrix $\underline{K}$. It is multiplied by the states $\underline{x}(t)$ to produce the control signals $\underline{u}(t)$ according to the linear-state-variable feedback (LSVF) control law.

$$\underline{u}(t) = -\underline{K}\,\underline{x}(t). \tag{10}$$

The LQR feedback gain matrix $\underline{K}$ is defined by

$$\underline{K} = \underline{R}^{-1}\underline{G}^{T}\underline{S}, \tag{11}$$

where the symmetric N × N matrix $\underline{S}$ is the positive definite solution of the matrix algebraic Riccati equation (ARE)

$$\underline{S}\,\underline{F} + \underline{F}^{T}\underline{S} - \underline{S}[\underline{G}\,\underline{R}^{-1}\underline{G}^{T}]\underline{S} + \underline{Q} = 0. \tag{12}$$

The closed-loop poles that characterize the transient response of the controlled system are the roots of the closed-loop characteristic equation

$$\text{Determinant}[s\underline{I} - (\underline{F} - \underline{G}\,\underline{K})] = 0. \tag{13}$$

In this classical optimal control problem, the LQR matrices $\underline{F}$, $\underline{G}$, $\underline{Q}$ and $\underline{R}$ are specified by the control engineer and $\underline{x}(t)$ is the sensed state-vector. To compute $\underline{K}$ and hence $\underline{u}(t)$ requires three steps:

(i) Solve (12) for the optimal return matrix $\underline{S}$.

(ii) Use $\underline{S}$ and (11) to compute the LQR feedback gain matrix $\underline{K}$.

(iii) Use (10) to determine the control signals $\underline{u}(t)$.

In Section 4, we demonstrate how to achieve these operations on the IOP of Figure 1.

4. ARE AND LQR SOLUTIONS

To solve the matrix ARE on the vector-matrix IOP of Figure 1 requires modification of (12) into a problem involving the solution of a system of linear algebraic equations. We achieve this step by examining the Kleinman algorithm [10]. This algorithm determines $\underline{S}$ in (12) by finding successively the unique positive definite solutions $\underline{S}(k)$ of the linear matrix equation

$$\underline{S}(k)\underline{F}(k) + \underline{F}^{T}(k)\underline{S}(k) + \underline{S}(k-1)\{\underline{G}\,\underline{R}^{-1}\underline{G}^{T}\}\underline{S}(k-1) + \underline{Q} = \underline{0}, \tag{14}$$

where k = 1,2,... is the iteration number and

$$\underline{F}(k) \triangleq \underline{F} - [\underline{G}\,\underline{R}^{-1}\underline{G}^{T}]\underline{S}(k-1). \tag{15}$$

In 1968, Kleinman showed that as $k \longrightarrow \infty$, the iterate $\underline{S}(k)$ approaches the positive definite solution $\underline{S}$ of the ARE. To solve (14) on the vector-matrix IOP, we first vectorize (14). We achieved this by converting each matrix in (14) into a vector according to the lexographic ordering of the elements of the matrix. For example, we described the vectorized version of the M × N matrix $\underline{H}$ by the column vector

$$\underline{C}[H] = [h_{11}h_{12}\ldots h_{1N}h_{21}h_{22}\ldots h_{2N}\ldots\ldots h_{M1}h_{M2}\ldots h_{MN}]^{T}$$

with M · N elements.

In our notation, we write the vectorized version of the Kleinman algorithm of (14) in terms of the column vectors $\underline{C}[\cdot]$ as

$$\underline{F}[\underline{F}(k)]\underline{C}[\underline{S}(k)] = -\underline{C}[\underline{S}(k-1)\{\underline{G}\,\underline{R}^{-1}\underline{G}^{T}\}\underline{S}(k-1)] - \underline{C}[\underline{Q}], \tag{16}$$

for k = 1,2,.... In (16), $\underline{F}[\underline{F}(k)]$ is a special two-dimensional formatted $N^2 \times N^2$ mask of $\underline{F}(k)$ in (15). The term $\underline{F}[\underline{F}(k)]\underline{C}[\underline{S}(k)]$ on the left-hand side of (16) is the vectorization of the linear term $[\underline{S}(k)\underline{F}(k) + \underline{F}^{T}(k)\underline{S}(k)]$ in (14). The first-term on the right-hand side of (16) is the vectorization of the (k - 1)-th iterate of the quadratic term $[\underline{S}(k-1)[\underline{G}\,\underline{R}^{-1}\underline{G}^{T}]\underline{S}(k-1)]$ in (14) and $\underline{C}[\underline{Q}]$ is the vectorization of the state weighting matrix $\underline{Q}$.

For N = 3, the vectorization of the linear term in (14) is the vector-matrix product

$$\underline{F}[\underline{F}(k)]\underline{C}[\underline{S}(k)] = \underbrace{\begin{bmatrix} \underline{F}^T(k) + f_{11}(k)\underline{I} & f_{21}(k)\underline{I} & f_{31}(k)\underline{I} \\ f_{12}(k)\underline{I} & \underline{F}^T(k) + f_{22}(k)\underline{I} & f_{32}(k)\underline{I} \\ f_{13}(k)\underline{I} & f_{23}(k)\underline{I} & \underline{F}^T(k) + f_{33}(k)\underline{I} \end{bmatrix}}_{\underline{F}[\underline{F}(k)]} \underbrace{\begin{bmatrix} s_{11}(k) \\ s_{12}(k) \\ s_{13}(k) \\ s_{21}(k) \\ s_{22}(k) \\ s_{23}(k) \\ s_{31}(k) \\ s_{32}(k) \\ s_{33}(k) \end{bmatrix}}_{\underline{C}[\underline{S}(k)]} \tag{17}$$

where $\underline{C}[\underline{S}(k)]$ is the column vectorization of the optimal return matrix $\underline{S}$ at the k-th iteration of the Kleinman algorithm and the matrix $\underline{I}$ in $\underline{F}[\underline{F}(k)]$ is the $N \times N$ identity matrix. The $N^2 \times N^2$ matrix mask $\underline{F}[\underline{F}(k)]$, which is computed according to (15), displays a block structure. There are N^2 matrix blocks in $\underline{F}[\underline{F}(k)]$; each block is an $N \times N$ matrix. The transpose $\underline{F}^T(k)$ of $\underline{F}(k)$ is replicated along the main diagonal blocks of $\underline{F}[\underline{F}(k)]$. Furthermore, the lexographic ordering of the elements of $\underline{F}^T(k)$ appears along the main diagonals of the matrix blocks. The remaining $[N(N-1)]^2$ of the N^4 elements of $\underline{F}[\underline{F}(k)]$ are zero. Thus computing and formatting the elements of $\underline{F}[\underline{F}(k)]$ are straightforward.

Through our systematic vectorization of (14) we have converted the Kleinman algorithm into repeated problems involving the solutions of systems of N^2 linear algebraic equations in the form of (16). We rewrite our modified iterative Kleinman algorithm in the form

$$\underline{H}(k)\underline{x}(k) = \underline{y}(k), \tag{18}$$

where:

$$\underline{H}(k) = \underline{F}[\underline{F}(k)] \tag{19}$$

$$\underline{x}(k) = \underline{C}[\underline{S}(k)] \tag{20}$$

$$\underline{y}(k) = -\underline{C}[\underline{S}(k-1)\{\underline{G}\,\underline{R}^{-1}\underline{G}^T\}\underline{S}(k-1)] - \underline{C}[\underline{Q}] \tag{21}$$

and $k = 1,2,\ldots$ is the iteration index. We can now solve the vector-matrix equation (18) and hence the matrix ARE (12) for $\underline{S}$ on the IOP of Figure 1.

To solve (16) and (18), we initialize $\underline{S}(0)$ and set the iterative index k for the Kleinman algorithm equal to 1. At each iteration k of (16), we calculate $\underline{F}(k)$ in (15), format $\underline{H}(k) = \underline{F}[\underline{F}(k)]$ as in (17) and (19) and compute $\underline{y}(k)$ as in (21). We then enter an inner Richardson iterative loop (with iteration index j) in which we use the previous iteration $\underline{S}(k-1)$ to solve (18) for the next iterate $\underline{S}(k)$ of $\underline{S}$. We thus see that the solution of (16) for $\underline{S}$ involves <u>two</u> iterative loops:

(i) An inner loop (index j) in which the Richardson algorithm of (4) is used to solve (18) for $\underline{S}(k)$ from $\underline{S}(k-1)$, and

(ii) An outer loop (index k) in which our modified Kleinman algorithm in (16) is used to update $\underline{F}(k)$ and $\underline{y}(k)$ and format $\underline{F}[\underline{F}(k)]$ for the next inner loop as in (15), (19), and (21).

To solve the matrix ARE, therefore, a new mask $\underline{H}(k) = \underline{F}[\underline{F}(k)]$ in (17) must be calculated at each outer (Kleinman algorithm) loop iteration k and placed at P_2 in the IOP of Figure 1. We thus require a real-time, adaptive and reuseable mask at P_2. Real-time spatial light modulators such as the CCD-addressed liquid crystal light valve [13] can provide such a real-time P_2 mask.

5. EXPERIMENTAL DEMONSTRATIONS

To illustrate the IOP, we solve a system of ten linear algebraic equations in which the exogenous vector is $\underline{y} = [1\ 1\ 1\ 1\ 1\ 1\ 1\ 1\ 1\ 1]$ and the matrix $\underline{H}$ is the lower-triangular 10×10 matrix

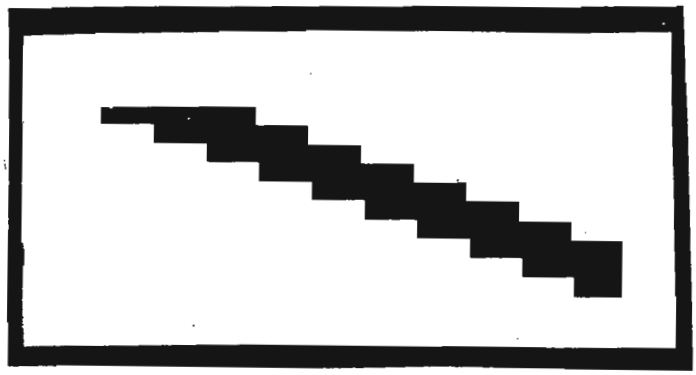

FIGURE 4. Reverse-contrast photograph of the B mask corresponding to (22)

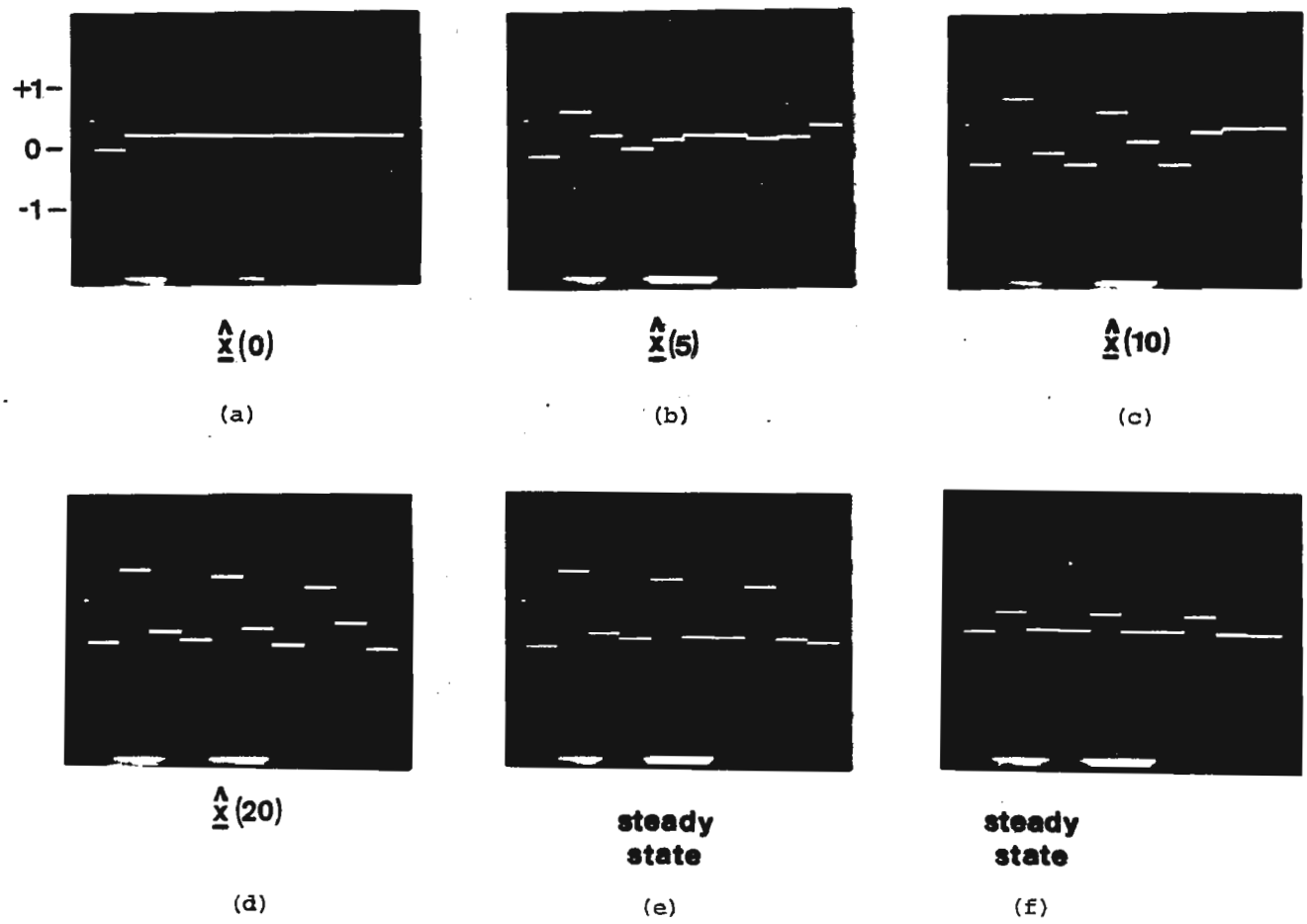

FIGURE 5. Real-time IOP outputs x(j) at selected iterations j

$$\underline{H} = \begin{bmatrix} 1 & 0 & 0 & 0 & 0 & 0 & 0 & 0 & 0 & 0 \\ 1 & 1 & 0 & 0 & 0 & 0 & 0 & 0 & 0 & 0 \\ 1 & 1 & 1 & 0 & 0 & 0 & 0 & 0 & 0 & 0 \\ 0 & 1 & 1 & 1 & 0 & 0 & 0 & 0 & 0 & 0 \\ 0 & 0 & 1 & 1 & 1 & 0 & 0 & 0 & 0 & 0 \\ 0 & 0 & 0 & 1 & 1 & 1 & 0 & 0 & 0 & 0 \\ 0 & 0 & 0 & 0 & 1 & 1 & 1 & 0 & 0 & 0 \\ 0 & 0 & 0 & 0 & 0 & 1 & 1 & 1 & 0 & 0 \\ 0 & 0 & 0 & 0 & 0 & 0 & 1 & 1 & 1 & 0 \\ 0 & 0 & 0 & 0 & 0 & 0 & 0 & 1 & 1 & 1 \end{bmatrix} . \qquad (22)$$

Since the largest element $\bar{h} = 1$ and the smallest element $\underline{h} = 0$, the difference $(\bar{h} - \underline{h}) = 1$. Consequently, the scaled and biased matrix $\underline{B}$ in (5) is identical to $\underline{H}$. The reverse-contrast photograph of the actual mask which was drawn on graphic-arts masking film and photoreduced onto 35 mm film is shown in Figure 4. Since the ten eigenvalues of $\underline{H}$ are all equal to one, the Richardson algorithm (4) will converge for all values of the acceleration parameter ω satisfying $0 < |1 - \omega| < 1$. To observe the gradual convergence of the IOP, we selected the value $\omega = 0.25$ for the experiment. The experimental results at iterations $j = 0$, 5, 10 and 20 and the steady-state solution are shown in Figures 5a - 5e. Variations across the outputs are caused by the LED array, fiber-optic element and detector non-uniformities which were not electronically corrected in this initial experiment. Reducing the vector $\underline{y}$ by a factor of four to reduce the accuracy of the microprocessor to that of the optical system (≈ 6 bits) improves the appearance of the steady-state solution as shown in Figure 5f.

6. SUMMARY AND CONCLUSIONS

We have introduced, described and fabricated a general-purpose optical processor that is capable of solving systems of linear algebraic equations. This iterative optical processor (IOP) is capable of operating on large input vectors and matrices (500 element input and detector arrays and a 500 × 500 element dynamic mask are feasible) in parallel at very high cycle times (a vector-matrix multiplication every 1 nsec is within the realm of possibility). Many data processing problems can be formulated as vector-matrix equations. In this paper, we have chosen the solution of the algebraic Riccati equation and the linear quadratic regulator problem of modern control engineering. We have modified the conventional algorithms and shown how the IOP can be used for these applications. This process has extended the repertoire of IOP operations to include the solution of nonlinear matrix equations. The application of the IOP technique to the LQR control of the F100 turbofan jet engine has been presented, associated new algorithms have been developed, and initial experimental demonstrations of the system have been included. Our present research on this system is directed toward finalizing the details of implementation of the Kleinman and Richardson algorithms on the IOP and analyzing the error sources in the system.

ACKNOWLEDGEMENTS

We thank NASA-Lewis Research Center for support of this work (Grant NAG 3-5) and to Robert Baumbick and James Seilers for providing us with guidance on F100 control applications.

REFERENCES

1. G.L. Poppel, "Analysis and Preliminary Design of an Optical Digital Tip Clearance Sensor for Propulsion Control," General Electric Co. Evendale, OH 45215, NAS3-21006, September 1978.

2. W.H. Glenn, et al., "Analysis and Preliminary Design of Optical Sensors for Propulsion Control," United Technologies Research Center, East Hartford, CT 06108, NAS3-21004, March 1979.

3. D. Psaltis, D. Casasent and M. Carlotto, "Iterative Color-Multiplexed, Electro-Optical Processor," Optics Letters, Vol. 4, No. 11, pp. 348-350, November 1979.

4. R.L. DeHoff, et al., "F100 Multivariable Control Synthesis Program - Volume I: Development of F100 Control System," Systems Control, Inc., Palo Alto, CA 94304, AFAPL-TR-77-35, June 1977.

5. R.L. DeHoff, et al., "F100 Multivariable Control Synthesis Program - Volume I: Appendices A through K," Systems Control, Inc., Palo Alto, CA 94304, AFAPL-TR-77-35, June 1977.

6. M.K. Sain, J.L. Peczkowski and J.L. Melsa (editors), Alternatives for Linear Multivariable Control. Chicago: National Engineering Consortium, Inc., 1978.

7. A.E. Bryson and Y.C. Ho, Applied Optimal Control. Waltham, MA: Blaisdell Publishing Co., 1969, Chapter 5.

8. M. Athans (editor), "Special Issue on the Linear-Quadratic-Gaussian Estimation and Control Problem," IEEE Transactions on Automatic Control, Vol. AC-16, No. 6, December 1971.

9. D.M. Young, Iterative Solution of Large Linear Systems. New York: Academic Press, 1971, pp. 94 and 361-365.

Casasent 7

10. D.L. Kleinman, "On an Iterative Technique for Riccati Equation Compution," IEEE Transactions on Automatic Control, Vol. AC-13, No. 1, pp. 114-115, February 1968.
11. J. Goodman, A. Dias and L. Woody, "Fully Parallel, High Speed Incoherent Optical Method for Performing Discrete Fourier Transforms," Optics Letters, Vol. 2, No. 1, pp. 1-3, January 1978.
12. E. Kreyszig, Advanced Engineering Mathematics. John Wiley and Sons, Inc., New York, 1972, p. 686.
13. J. Grinberg, et al., "Liquid Crystal Electro-Optical Modulators for Optical Processing of Two-Dimensional Data," Society of Photo-Optical Instrumentation Engineers, Vol. 128, p. 253: Effective Utilization of Optics in Radar Systems, 1977.

Consent 8